Dispersive and global spherical optical model with a local energy approximation for the scattering of neutrons by nuclei from 1 keV to 200 MeV

B. Morillon and P. Romain
Commissariat à l'Énergie Atomique, DAM/DIF/DPTA/SPN, Boîte Postale 12, 91680 Bruyères-le-Châtel, France
(Received 8 March 2004; published 6 July 2004)

We present a global spherical optical model potential for neutrons with incident energies from 1 keV up to 200 MeV containing dispersive terms and a local energy approximation. A comprehensive database for spherical or quasispherical nuclei covering the mass range $24 \leqslant A \leqslant 209$ is used to automatically search on all parameters. A good representation of the entire data set is obtained when both volume and surface potentials share the same energy-independent geometry.

DOI: 10.1103/PhysRevC.70.014601 PACS number(s): 24.10.Ht

I. INTRODUCTION

Over the last 50 years, the nuclear optical model has been extensively applied to analyze the scattering of protons and neutrons by nuclei. Nowadays, several global optical models are available to predict the total nucleon cross sections and angular distributions for many nuclei over a wide range of energies such as the well-known global optical models of Rapaport *et al.* [1], Walter-Guss [2], Varner *et al.* [3], Madland [4], and Koning-Delaroche [5]. Nevertheless, there is no global potential including dispersion relations [6] that links the real and imaginary parts of the nuclear potential. The dispersive optical model (DOM) provides an additional constraint to reduce the ambiguities when determining the parameters of the optical model.

The purpose of this contribution is to build a global dispersive spherical optical model for neutrons with incident energies from 1 keV up to 200 MeV. At Bruyères-le-Châtel, we have already applied the DOM to many neutron-nucleus scattering systems, however, until now we have never tried to build a global one. Because in all our past studies, the local energy approximation of Perey-Buck [7] was used with great success we have decided to include it in our global DOM.

The paper is structured as follows. In Sec. II, we provide a description of the DOM with the functional forms of the energy dependencies of the real, imaginary, and spin-orbit potentials. Section III describes our procedure for searching the parameters of the optical model and the resulting DOM potential is discussed in Sec. IV. Finally, our conclusions are given in Sec. V.

II. OPTICAL MODEL

The optical model potential we use can be written as

$$U(r,E) = [V_V(E) + iW_V(E)]f(r,R_V,a_V) + [V_S(E) + iW_S(E)]g(r,R_S,a_S) + [V_{SO}(E) + iW_{SO}(E)] \times \left(\frac{h}{m_\pi c}\right)^2 \frac{1}{r} g(r,R_{SO},a_{SO}) \mathbf{l} \cdot \sigma, \quad (1)$$

where $V_{V,S,SO}$ and $W_{V,S,SO}$ are the real and imaginary terms of the volume-central (V), surface-central (S), and spin-orbit (SO) potentials. The volume shape f is a Woods-Saxon form factor while the surface shape g is proportional to its first derivative:

$$f(r,R,a) = \frac{1}{1 + \exp[(r-R)/a]},$$

$$g(r,R,a) = -4a \frac{d}{dr} f(r,R,a).$$

Initially the volume, surface, and spin-orbit shapes do not share the same geometrical parameters (radius R and diffuseness a). Note also that these parameters ($R_{V,S,SO}$, $a_{V,S,SO}$) are independent of energy.

In the dispersion relations treatment [6], the real V and imaginary W volume potentials are connected by a dispersion relation

$$V(E) = V_{HF}(E) + \Delta V(E),$$

$$\Delta V(E) = \frac{P}{\pi} \int_{-\infty}^{+\infty} \frac{W(E')}{E' - E} dE'. \quad (2)$$

As usual, P denotes the principal value of the integral and $V_{HF}(E)$ the Hartree-Fock contribution to the mean field.

A. Imaginary potentials

The energy dependence of the volume imaginary term is taken to be the form first suggested by Brown and Rho [8]:

$$W_V(E) = \frac{A_V (E - E_F)^2}{(E - E_F)^2 + B_V^2}. \quad (3)$$

For the surface imaginary term, we use an energy dependence suggested by Delaroche *et al.* [9] which modifies the Brown-Rho shape by an exponential falloff

$$W_S(E) = \frac{A_S (E - E_F)^2}{(E - E_F)^2 + B_S^2} \exp[-C_S(E - E_F)]. \quad (4)$$

The values of A_V, B_V, A_S, B_S, C_S are to be determined by fitting experimental data.

Throughout the present paper, we use a imaginary spin orbit energy dependence very close to those of Koning *et al.* [5]:

$$W_{\mathrm{SO}}(E) = \frac{-3(E-E_F)^2}{(E-E_F)^2+160^2}. \tag{5}$$

All the energy dependencies of the imaginary potential are symmetric about the Fermi energy $E_F = -[S_n(Z,N)+S_n(Z,N+1)]/2$.

B. Real potentials

A realistic parametrization of the Hartree-Fock potential was postulated by Perey and Buck [7]. In their work, the nonlocality of $V_{\mathrm{HF}}(\mathbf{r},\mathbf{r}')$ has a Gaussian form

$$V_{\mathrm{HF}}(\mathbf{r},\mathbf{r}') = V(\mathbf{r})\exp(-|\mathbf{r}-\mathbf{r}'|^2/\beta^2),$$

where β is the nonlocality range. The local energy approximation then yields [7]

$$V_{\mathrm{HF}}(E) = V_{\mathrm{HF}}\exp(-\mu\beta^2[E-V_{\mathrm{HF}}(E)]/2\hbar^2), \tag{6}$$

where μ is the reduced mass of the system. Johnson *et al.* [10] used this form in their dispersive optical-model analysis about ^{40}Ca. We have also tried such a parametrization in our work, however, better results were obtained, especially beyond 100 MeV, by using the form of Romain *et al.* [11]:

$$V_{\mathrm{HF}}(E) = V_{\mathrm{HF}}\exp(-\mu\beta^2[E-V_{\mathrm{HF}}(E)]/2\hbar^2) \times \exp(+4\mu^2\gamma^2[E-V_{\mathrm{HF}}(E)]^2/\hbar^4). \tag{7}$$

The total real volume potential $V_V(E) = V_{\mathrm{HF}}(E) + \Delta V_V(E)$ is obtained from Eqs. (2) and (7) using the imaginary volume form (3) in the dispersion relation. The nonlocality ranges β and γ will be specified in the analysis of available experimental data. The total real surface potential $V_S(E)$ is equal to the surface dispersive contribution $\Delta V_S(E)$ calculated from imaginary surface potential defined by Eq. (4).

As we have done for the imaginary spin orbit component, the real spin orbit is close to that of Koning *et al.* [5]:

$$V_{\mathrm{SO}}(E) = 6\ \exp[-0.004(E-E_F)] + \Delta V_{\mathrm{SO}}(E).$$

Even if it is difficult to prove the existence of the imaginary spin orbit potential we connected it to the real spin orbit potential by a dispersion relation. Analytical and numerical solutions of dispersion relations may be found in Quesada *et al.* [12] and Capote *et al.* [13], assuming that $W(E)$ is symmetric about the Fermi energy.

III. OPTIMIZATION OF OPTICAL MODEL PARAMETERS

Our nonlocal dispersive and spherical optical model is now specified. For each nucleus, a set of fourteen parameters must be determined: three radii $R_{V,S,\mathrm{SO}}$, three diffuseness parameters $a_{V,S,\mathrm{SO}}$, nonlocality ranges β and γ as well as the depth V_{HF}, and the imaginary potentials parameters A_V, B_V, A_S, B_S, C_S. To that aim, an automatic χ^2 search on all of these parameters is now included in the NUCLEON code [14] (NUCLEON was first written to investigate the nucleon-nucleon interactions). This code provides a numerical integration of the radial Schrödinger equation using the Numerov's method [15], which is also used by the ECIS code [16]. Relativistic kinematics without Dirac formalism is also included as it is mentioned in the miscellaneous topics of the ECIS report [16].

To optimize the optical model parameters for a nucleus, two quantities can be calculated

$$\chi^2_{\mathrm{XS}} = \sum_{i=1}^{N_{\mathrm{XS}}}\left[\frac{\sigma_{T\,i}^{\mathrm{exp}}-\sigma_{T\,i}^{\mathrm{cal}}}{\Delta\sigma_{T\,i}^{\mathrm{exp}}}\right]^2$$

and

$$\chi^2_{\mathrm{AD}} = \sum_{i=1}^{N_{\mathrm{AD}}}\sum_{j=1}^{N_{\mathrm{AD}i}}\left[\frac{\sigma_i^{\mathrm{exp}}(\theta_j)-\sigma_i^{\mathrm{cal}}(\theta_j)}{\Delta\sigma_i^{\mathrm{exp}}(\theta_j)}\right]^2,$$

the first one (χ^2_{XS}) for the total cross sections and the second one (χ^2_{AD}) for the elastic angular distributions. Here, σ_T is the total cross section, $\sigma(\theta)$ the differential elastic cross section ("exp" stands for experimental and "cal" for calculated values) and $\Delta\sigma$ is the experimental uncertainty. For each nucleus N_{XS} is the number of experimental total cross section data points, N_{AD} is the number of experimental angular distributions, and $N_{\mathrm{AD}\,i}$ is the number of data points for a given experimental angular distribution i.

The determination of the parameters of the global optical model potential is possible if and only if the experimental data set is wide enough. Thus our search procedure makes extensive use of the comprehensive Koning and Delaroche database [5]. In the range from 1 keV to 200 MeV, the experimental data of the following twenty nuclei are used to determine our parameters: $^{\mathrm{nat}}$Mg, ^{27}Al, $^{\mathrm{nat}}$Si, $^{\mathrm{nat}}$S, $^{\mathrm{nat}}$Ca, $^{\mathrm{nat}}$Ti, $^{\mathrm{nat}}$Cr, $^{\mathrm{nat}}$Fe, $^{\mathrm{nat}}$Ni, $^{\mathrm{nat}}$Cu, ^{89}Y, ^{90}Zr, ^{93}Nb, $^{\mathrm{nat}}$Mo, $^{\mathrm{nat}}$Sn, $^{\mathrm{nat}}$Ce, ^{197}Au, $^{\mathrm{nat}}$Hg, ^{208}Pb, ^{209}Bi.

Using a grid method in the multidimensional "chi-squared space," the NUCLEON code searches optimal parameters either for all nuclei in the same run owing to parallel computers or for a subset of nuclei. The starting set of parameters a_V, R_V, A_V, B_V, a_S, R_S, A_S, B_S, C_S, a_{SO}, R_{SO} are those of the global neutron optical model of Koning and Delaroche [5] and the Romain's unpublished previous investigations for the parameters β, γ, and V_{HF}.

In the Koning and Delaroche global optical model, the geometrical parameters a and $R = r_0 A^{1/3}$ are different for the volume, surface, and spin-orbit potentials. On one hand, the reduced radius r_V of the volume potential increases with nuclear mass when the reduced radius r_S for the surface potential decreases to a value close to r_V for heavy nuclei (Fig. 1). On the other hand, diffuseness parameters for both volume and surface potentials decrease linearly with mass giving two different slopes for the Koning and Delaroche potential (Fig. 2). The reduced radius r_{SO} for the real spin-orbit potential increases with mass whereas the diffuseness a_{SO} has a constant value. In that way we use these variations for the geometrical parameters as a starting point for the χ^2 search. Thus our starting optical model mentioned in Eq. (1) has different radii and diffuseness for the volume, surface, and spin-orbit potentials.

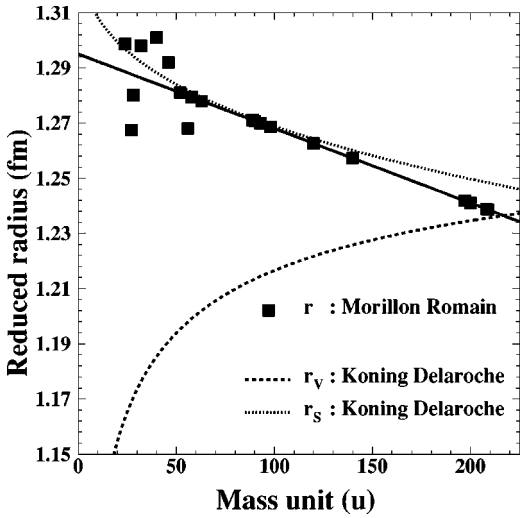

FIG. 1. Reduced radii of our global optical model. The square symbols represent the optimal reduced radii and the solid curve the global parametrization ($r_0 = 1.295 - 2.7 \times 10^{-4}$A). The long-dashed curve and short-dashed curves correspond to the volume and surface reduced radii of Koning and Delaroche.

The first step to construct our optical model is to specify the real part of the potential. That is to say the nonlocality ranges β and γ, the depth V_{HF}, the radii, and the diffuseness of the volume and surface potential are the free parameters. In the beginning, only the total cross sections are inserted in the χ^2 search since these data are more sensitive to the real potential. After an automatic χ^2 search on 20 processors at once, we obtain the values of the seven parameters for every nuclei of our experimental data set. Looking into the variations of these results with the energy, the atomic mass, or the asymmetry parameter $(N-Z)/A$ (all parameters change from nucleus to nucleus), we find simple energy or mass functional forms to describe the seven parameters. The main surprise of this first search is the mass variations of the radii. The best fit to the total cross sections is reached when both volume and surface shapes share similar potential radii. In view of that result, we try to search a shape shared by the volume and surface potentials, that is to say, the functional forms of the radii and of the diffuseness parameters are the same for the volume, surface and spin-orbit potentials. Starting from the new functional forms, the work is performed by iterative computations to obtain the parameters of the real part of the potential.

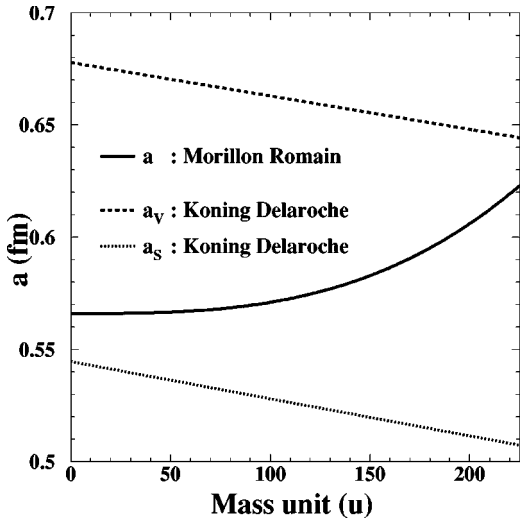

FIG. 2. Diffuseness parameter of our global optical model. The solid curve represents the global parametrization ($a = 0.566 + 5 \times 10^{-9}$A^3). The long-dashed and short-dashed curves correspond to the volume and surface diffuseness parameters of Koning and Delaroche.

TABLE I. Reduced radii for nuclei lighter than nickel. $R = r_0 A^{1/3}$.

Nucleus	r_0(fm)	Nucleus	r_0(fm)
^{24}Mg	1.299	^{40}Ca	1.301
^{27}Al	1.267	^{46}Ti	1.292
^{28}Si	1.280	^{56}Fe	1.268
^{32}S	1.298		

The second step is to fix the imaginary part. For each nucleus, five parameters are needed (A_V, B_V, A_S, B_S, C_S). The elastic differential cross sections are then inserted in the χ^2 search and the functional forms are obtained for the five parameters. At low energies, a compound nucleus contribution to the elastic channel must be calculated from statistical model and added to the shape elastic cross section. The TALYS code (a new reaction code under development [17]) provides such calculations for our new neutron optical model with width fluctuation corrections as modified by Moldauer [18]. Transmission coefficients for proton, deuteron, triton, and α particles in the exit channels are derived from the nucleon potentials of Koning and Delaroche [5] using Watanabe's folding approach [19].

Finally, a global χ^2 optimization using the total and differential cross sections was carried out to fine-tune the optical model parameters. $(N-Z)/A$ dependence of any parameters was not needed in this study. In fact this is a moderately surprising result when building a global optical potential for just one kind of incident particle, a neutron in our case.

A. Geometrical parameters radius and diffuseness

For nuclei heavier than iron the reduced radius is well approximated by the following parametrization:

$$r_0 = 1.295 - 2.7 \times 10^{-4}\, A(\mathrm{fm}). \tag{8}$$

The reduced radius r_0 decreases when the nuclear mass A increases as a result similar to the one found by Chiba *et al.* [20]. For lighter nuclei, a better agreement between the calculated and experimental total cross sections is obtained by using the individual radii given in Table I (the improvement is particularly huge for aluminium and iron). These values are plotted in Fig. 1. The square symbols represent the optimal reduced radii, and the solid curve represents the previous parametrization. Our reduced radius parametrization is close to the surface radius of Koning and Delaroche also plotted in Fig. 1.

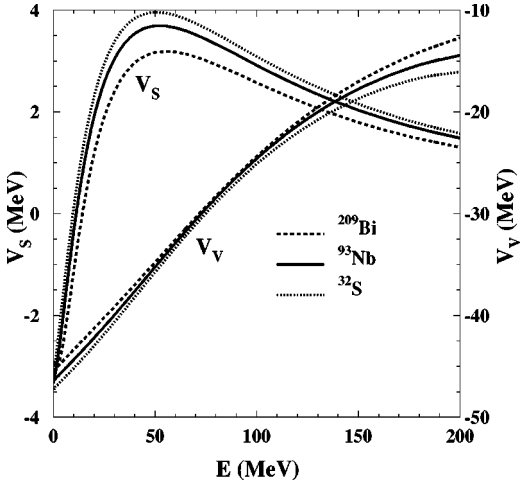

FIG. 3. Depths of volume $[V_V(E)=V_{\mathrm{HF}}(E)+\Delta V_V(E)]$ and surface $[V_S(E)=\Delta V_S(E)]$ real potentials for ^{32}S, ^{93}Nb, and ^{209}Bi. The scale for the surface potential is on the left and on the right for the volume potential.

The diffuseness parameter which is also the same for the volume and surface potential increases with mass as

$$a = 0.566 + 5 \times 10^{-9} \mathrm{A}^3(\mathrm{fm}).$$

The diffuseness parameters of the volume (long-dashed curve) and surface (short-dashed curve) potentials from Koning and Delaroche surround our parametrization (solid line) as can be seen in Fig. 2.

B. Real potentials

The nonlocality range β and the depth V_{HF} show very little variation with mass. The fitting procedure leads to the following values:

$$V_{\mathrm{HF}} = -82.8 \text{ MeV}, \quad \beta = 1.114 \text{ fm}.$$

We note that our nonlocality range β is similar to the value 1.19 adopted by Johnson and Mahaux [10]. The nonlocality range γ decreases slowly with mass as

$$\gamma = 0.233 - 2 \times 10^{-4} \mathrm{A(fm)}.$$

Energy dependencies of the depths of the real-volume potential (Hartree-Fock plus volume dispersive contribution ΔV_V) as well as the surface dispersive contribution ΔV_S are shown in Fig. 3 for three nuclei (^{32}S, ^{93}Nb, and ^{209}Bi). The depth of the real volume and surface potentials for niobium always stands between the lighter and the heavier nuclei.

C. Imaginary potentials

As the C_S and B_S parameters of the surface imaginary potential [see Eq. (4)] show little variation with mass, we adopt the average results of our fitting procedure

$$B_S = 11.5 \text{ MeV}, \quad C_S = 0.023 \text{ MeV}^{-1}.$$

On the other hand, the depth A_S of the surface imaginary potential increases with mass as

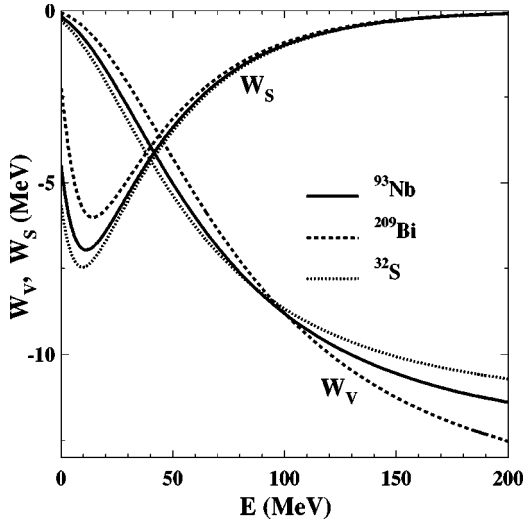

FIG. 4. Depths of volume $[W_V(E)]$ and surface $[W_S(E)]$ imaginary potentials for ^{32}S, ^{93}Nb, and ^{209}Bi

$$A_S = -15 + 0.018 \text{ A(MeV)}.$$

For the volume imaginary potential the mass dependence of the parameters A_V and B_V are the following:

$$A_V = -11.21 - 0.017 \text{ A(MeV)},$$

$$B_V = 62 + 0.12 \text{ A(MeV)}.$$

Energy dependencies of the depths of the imaginary volume and surface potentials are shown in Fig. 4 for the same three nuclei (^{32}S, ^{93}Nb, and ^{209}Bi). The depth of the imaginary surface potential for niobium is always located between the lighter and heavier nuclei even when the imaginary volume potential presents astonishing variations: the greatest volume contribution is for the lightest nucleus below 100 MeV and for the heaviest nucleus above 100 MeV.

IV. RESULTS AND COMPARISONS

It is not easy to present all the comparisons of our results with experimental data. In addition, it is important to compare our results with other global optical models. Koning and Delaroche did it for the global neutron optical model [5]. They have compared their results with the well-known global optical models of Wilmore-Hodgson, Rapaport *et al.*, Varner *et al.*, Walter-Guss, and Madland. Owing to χ^2 comparisons they found that their new global neutron optical model performed better than each of the previous models. In that way and to show concise comparisons, we only present χ^2 results for our global optical model and for the global optical model of Koning and Delaroche.

The $\chi^{2\mathrm{KD}}_{\mathrm{XS}}$ and $\chi^{2\mathrm{KD}}_{\mathrm{AD}}$ values calculated with the global optical model of Koning and Delaroche relative to our results noted $\chi^{2\ \mathrm{MR}}_{\mathrm{XS}}$ and $\chi^{2\ \mathrm{MR}}_{\mathrm{AD}}$ are listed in Table II for every nucleus of the database. The first column shows the symbol of the nucleus for the experimental data whereas the second one shows the calculated nucleus. In the third and fifth column the relative χ^2 for the angular distributions and the total cross

TABLE II. Comparison of our global optical model for the neutron with the global potential of Koning and Delaroche.

Exp.	Cal.	$\chi^{2KD}_{AD}/\chi^{2MR}_{AD}$	Total	$\chi^{2KD}_{XS}/\chi^{2MR}_{XS}$	Total
Mg	^{24}Mg	1.33	1.33	0.92	0.92
^{27}Al	^{27}Al	1.04	1.15	2.06	1.42
Si	^{28}Si	0.90	1.07	1.03	1.28
S	^{32}Si	0.93	1.02	1.22	1.26
^{40}Ca	^{40}Ca	0.77	0.98	0.98	1.21
Ti	^{46}Ti	0.82	0.97	2.83	1.46
Cr	^{52}Cr	0.89	0.96	3.82	1.77
Fe	^{56}Fe	1.03	0.96	1.02	1.68
Ni	^{58}Ni	1.14	0.98	1.20	1.63
Cu	^{63}Cu	1.13	0.99	1.07	1.58
^{89}Y	^{89}Y	1.00	0.99	1.69	1.59
^{90}Zr	^{90}Zr	1.04	1.00	2.04	1.63
^{93}Nb	^{93}Nb	0.83	0.98	1.68	1.63
Mo	^{98}Mo	1.01	0.98	1.14	1.60
Sn	^{120}Sn	0.79	0.97	2.78	1.68
Ce	^{140}Ce	1.02	0.97	3.60	1.77
^{197}Au	^{197}Au	1.11	0.98	0.83	1.71
Hg	^{200}Hg	1.26	0.98	4.29	1.85
^{208}Pb	^{208}Pb	1.09	0.99	1.04	1.80
^{209}Bi	^{209}Bi	1.05	**1.00**	1.06	**1.76**

sections are listed for every nucleus. The fourth and the sixth column (noted total) show the total cumulative relative χ^2 weighted by the number of measurements.

The main improvement is for the total cross sections. The χ square improves by 76%. Our global DOM provides a very good description of the total cross sections from 1 keV to 200 MeV as illustrated in Fig. 5 for S, ^{93}Nb, and ^{209}Bi. To calculate the cross sections for natural elements lighter than nickel (for instance, sulfur) one has to determine the reduced radius of each isotope. That can be done from the reduced radii of Table I owing to a straight line segment with the same slope as in the global parametrization [Eq. (8)]. The overall agreement with experimental data for natural elements is also very good.

As recorded in Table II, there is no improvement to the potential of Koning and Delaroche to the global χ^2 for the elastic angular distributions. Although the angular distributions are in phase over the whole energy and mass ranges, some deviations occur for backward minima in the Y-Nb region. That is the small price paid for using the same geometrical parameters for the real and imaginary potentials.

V. CONCLUSIONS

We have built a new global optical model potential for incident neutrons from 1 keV up to 200 MeV for spherical nuclei. The use of dispersion relations and the local energy approximation of Perey and Buck not only improves the quality of fit to the data but also leads to fewer parameters in the potential: the radii and the diffuseness parameters for the radial shape of the volume, surface, and spin-orbit potentials are the same. Functional forms describing our parameters are very simple. In that way the real potential, as well as the surface imaginary potential, are defined with only two linear functions of mass A (the nonlocality range γ and the parameter A_S). Our new global OMP provides a very good description of the total and differential elastic cross sections over a very broad energy domain for spherical nuclei. In that way the reaction cross section is also well defined and this new potential will provide better evaluations of partial cross sections for spherical nuclei. In view of the excellent agreement between predictions and experimental data for incident neutrons, we plan to build a global optical model for incident protons.

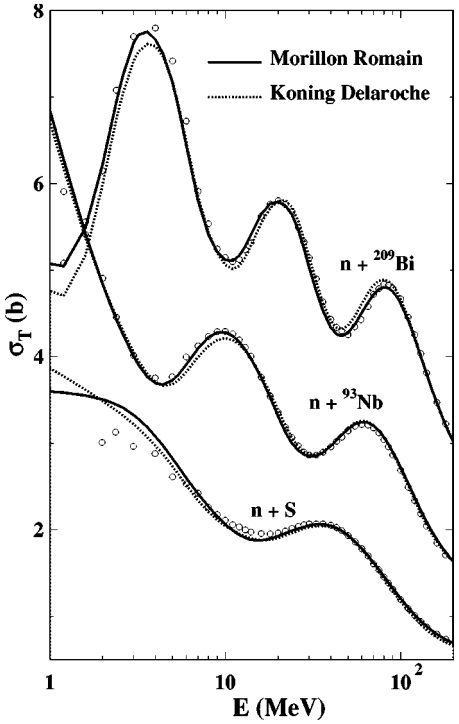

FIG. 5. Comparisons of measured (symbols) and calculated neutron total cross sections of S, ^{93}Nb, and ^{209}Bi. The short-dashed curve correspond to the global optical model of Koning and Delaroche and the solide curve to our global dispersive potential. The symbols are averaged on the various experimental values taken from the literature as described in Ref. [5].

ACKNOWLEDGMENTS

The authors would like to acknowledge R. Lazauskas and O. Bersillon for a critical reading of the manuscript.

[1] J. Rapaport, V. Kulkarni, and R. W. Finlay, Nucl. Phys. **A330**, 15 (1979).
[2] R. L. Walter and P. P. Guss, in *Proceedings of the International Conference on Nuclear Data for Basic and Applied Science*, edited by P. Young, R. Brown, G. Auchampaugh, P. Lisowski, and L. Stewart (Gordon and Breach, New York, 1986), Vol. 2, p. 1079.
[3] R. L. Varner, W. J. Thompson, T. L. McAbee, E. J. Ludwig, and T. B. Clegg, Phys. Rep. **201**, 57 (1991).
[4] D. G. Madland, in *Proceedings of a Specialists' Meeting on Preequilibrium Reactions, Semmering, Austria*, edited by B. Strohmaier (OECD Nuclear Energy Agency, Paris, 1988), p. 103.
[5] A. J. Koning and J. P. Delaroche, Nucl. Phys. **A713**, 231 (2003).
[6] C. Mahaux, H. Ngô, and G. R. Satchler, Nucl. Phys. **A449**, 354 (1986).
[7] F. G. Perey and B. Buck, Nucl. Phys. **32**, 353 (1962).
[8] G. E. Brown and M. Rho, Nucl. Phys. **A372**, 397 (1981).
[9] J. P. Delaroche, Y. Wang, and J. Rapaport, Phys. Rev. C **39**, 391 (1989).
[10] C. H. Johnson and C. Mahaux, Phys. Rev. C **38**, 2589 (1988).
[11] P. Romain and J. P. Delaroche, Proceedings of the Specialist' Meeting on the Nucleon Nucleus Optical Model up to 200 MeV, Bruyères-le-Châtel, 1996, available at http://www.nea.fr/html/sciences/om200.
[12] J. M. Quesada, R. Capote, A. Molina, M. Lozano, and J. Raynal, Phys. Rev. C **67**, 067601 (2003).
[13] R. Capote, A. Molina, and J. M. Quesada, J. Phys. G **27**, B15 (2001).
[14] B. Morillon (unpublished).
[15] A. Funk, H. V. von Geramb, and K. A. Amos, Phys. Rev. C **64**, 054003 (2003).
[16] J. Raynal, Notes on ECIS94, CEA Saclay Report No. CEA-N-2772, 1994.
[17] A. J. Koning, S. Hilaire, and M. Duijvestijn (unpublished).
[18] P. A. Moldauer, Nucl. Phys. **A344**, 185 (1980).
[19] S. Watanabe, Nucl. Phys. **8**, 484 (1958).
[20] S. Chiba, P. T. Guenther, R. D. Lawson, and A. B. Smith, Phys. Rev. C **42**, 2487 (1990).